Mechanism for dimerization and activation of the catalytic domain of the EGF receptor by the juxtamembrane segment

Natalia Jura, Nicholas F. Endres, Kate Engel, Sebastian Deindl, Rahul Das, Meindert H. Lamers, David E. Wemmer, Xuewu Zhang and John Kuriyan

Supplemental Data

Experimental Procedures

Multi-angle static light scattering

The N-terminally His-tagged kinase core or His-tagged JM-kinase constructs at 150 μM concentration were loaded on to a KW-803 size exclusion column preequilibrated in 20 mM TrisCl pH 8.0, 50 mM NaCl at a flow rate of 0.4 ml/min. The detection of eluted protein was carried out by a coupled 18-angle light scattering detector (Wyatt Technology Co.) and refractive index detector (Wyatt Technology Co.) with a data collection interval of 0.5 s. Data analysis was performed using ASTRA software (Wyatt Technology Co., Release 4.90.04)

Molecular dynamics

The model used for molecular dynamics included residues 672-967 from the structure of the active kinase domain of EGFR (PDB ID: 2GS6), in which the N-terminus was further extended until Ile 649 and contained the modeled JM-A helical fragment spanning the residues 665-653 and with Leu 655 at the *d* position of the heptad repeat. A separate peptide corresponding to the residues 649-685 of EGFR was docked on the C-lobe of the kinase to form a juxtamembrane latch interaction as seen in Her4 (Wood et al., 2008). The helix in this peptide, encompassing residues 665-653 forms a helical

dimer with the corresponding helix in the extension to the kinase domain, as described in the main manuscript. Three alanine residues were added at the N-termini of both peptide chains. The initial structure was immersed in a truncated octahedral cell of water molecules (TIP3P explicit water model). The water extended at least 8 Å past the surface of the protein molecule. 9 Cl^--counterions were added using the LEAP module of AMBER (version 9) (Case et al., 2006; Pearlman et al., 1995), with the parm96 force field (Cornell et al., 1995; Cornell et al., 1996). The SANDER module of AMBER was used to calculate the trajectories at constant temperature and pressure, SHAKE was used to constrain bonds to hydrogen (Ryckaert et al., 1977), and the particle mesh Ewald summation method was used to compute electrostatic interactions (Darden et al., 1993). The system was initially equilibrated for 100 ps, and positional harmonic restraints were applied for the first 50 ps, essentially as described earlier (Young et al., 2001). Four independent 10 ns-trajectories of the same starting model were generated using 16 xeon processors on an IBM X series 345 cluster and different random-number seeds for the initial assignment of velocities.

NMR analysis of 15 residue JM-A peptide

The JM-A peptide (residues 52-666) (H_3N^+-K_{652}RTLRRLLQERELVE_{666}-COO^-) was synthesized by solid phase method and the purity of the peptide was confirmed by mass spectrometry and NMR. The NMR sample was prepared by dissolving the JM-A peptide (2 mM final concentration) in 20 mM sodium phosphate buffer pH 6.8, 10% D_2O and 4% deutrated acetonitrile. The NMR data were acquired using Bruker AV900 MHz spectrometer fitted with a cryoprobe at 293K. All spin systems were assigned using chemical shifts from ^1H-^1H TOCSY, ^{13}C (natural abundance) HSQC, ^{13}C-^1H HSQC-

TOCSY experiments. The backbone sequential assignment was completed by NOE based sequential assignment methods using the ^{1}H-^{1}H NOESY experiment (Wüthrich, 1996). All NMR spectra were acquired with 2 s of recycle delay. The homonuclear 2D spectra were collected with spectral width of 1091Hz for both the dimension and 2048 and 512 complex points in the direct and indirect detected dimension, respectively. The natural abundance ^{1}H-^{13}C spectra were acquired with 2048 x 128 complex points and 10901 Hz and 20366Hz spectral width for direct and indirect detected dimension, respectively. The TOCSY spectra were acquired with 100 ms DIPSI mixing time with pulse strength of 10 kHz. The NOESY mixing time was set at 400 ms. The data were processed using Topspin (Bruker Inc.) and analyzed using Sparky 3.111 (Goddards and Kneller). The peak intensities were determined from the fit heights using Gaussian line fitting. The error in the fit height was estimated from the signal to noise ratio and propagated accordingly. The backbone amide resonances for the Lys 652 and Arg 653 could not be assigned due to chemical exchange, presumably with water.

To understand whether the JM-A peptide undergoes concentration dependent oligomerization, we studied the concentration dependent line broadening, detecting TOCSY transfer from the amides to the methyls of leucine and valine. Typically, due to the long coupling network between the amide and Hδ of leucine, or amide and Hγ of valine, the intensities of cross peaks for this region are very sensitive to broadening, presumably from a small population of oligomers. The TOCSY spectra were acquired with 0.2 mM, 0.5 mM and 2 mM peptide under identical conditions. The spectra were normalized using the T3Hγ-NH cross peak.

NMR analysis of a peptide containing two copies of the JM-A segment linked in tandem

A 35 residue peptide containing two copies of the JM-A segment with a five residue flexible spacer was synthesized by solid phase method and the purity of the peptide was confirmed by MS and NMR. The sequence of this peptide is H_3N^+-K_{652}RTLRRLLQERELVE$_{666}$-GSGSG-K_{652}RTLRRLLQERELVE$_{666}$$COO^-$, with the two JM-A segments denoted as Segment A and Segment B, respectively (Figure S7A). To probe potential interactions between the JM-A segments we labeled two specific residues with ^{15}N and one residue with ^{15}N and ^{13}C. The residues labeled are shown in bold with ^{15}N at the first and last leucine residues in the LRRLL motif in Segment A (Leu 655 and Leu 659 in the EGFR sequence). The residue labeled with ^{15}N and ^{13}C is the second glutamate in Segment A (Glu 663 in the EGFR sequence).

The NMR sample was prepared by dissolving the peptide to 0.5 mM in 50 mM deuterated acetate buffer pH 5.1 and 10% D_2O. The NMR data were acquired using a Bruker AV900 MHz spectrometer fitted with a cryoprobe at 293K. Spin systems were assigned using chemical shifts from a ^1H-^1H TOCSY experiment acquired with ^{15}N and ^{13}C decoupling, ^{15}N and ^{13}C HSQC, ^{13}C-^1H HSQC-TOCSY and ^{15}N-^1H HSQC-TOCSY experiments. The ^1H-^1H NOESY experiment was used to complete the backbone resonance assignment (Wüthrich, 1996). All homonuclear and heteronuclear experiments were acquired with recycle delay of 1.5 sec, and 2048 and 256 complex points for the direct and indirect detected dimension, respectively. The TOCSY spectra were acquired with 100 ms DIPSI mixing time with pulse strength of 10 kHz. The NOESY mixing time was set at 300 ms. The data were processed using Topspin (Bruker Inc.) and analyzed

using Sparky 3.111 (Goddards and Kneller). The backbone resonances for 23 amino acids of the JMA –JMA peptide could be assigned sequentially. The residues that could not be assigned due to spectral overlap in the first JM-A segment are Arg 653, Arg 657, Leu 658, Gln 660, Glu 661 and Arg 662. The terminal amide resonance for the Lys 652 could not be assigned due to chemical exchange, presumably with water. In the second JM-A segment the resonances for Arg 657, Leu 658, Leu 659, Gln 660, Glu 661 and Arg 662 could not be assigned due to spectral overlap.

The structure of the peptide was probed through ^{15}N-^{1}H HSQC –NOESY and ^{13}C-^{1}H HSQC – NOESY experiments. The NOESY spectra were acquired with 300 ms of mixing time, 2048 x 256 numbers of points in the direct and indirect detected dimensions and spectral width of 10901 Hz, 20366 Hz and 912 Hz for the ^{1}H, ^{13}C and ^{15}N dimensions, respectively.

Results

NMR Structural Analysis of 15 Residue JM-A Peptide

We used solution NMR experiments to analyze the conformation of an isolated peptide spanning the JM-A segment (residues 652-666). The secondary structure for the peptide was determined based on sequential connectivities inferred from the nuclear Overhauser effect (NOE) (Figure S2A and S2B), as well as Hα and Cα chemical shift values (Figure S2C and S2D). The presence of $d_{NN(i,\ i+1)}$ $d_{\alpha N(i,\ i+1)}$ $d_{\alpha N(i,\ i+3)}$ and $d_{\beta N(i,\ i+1)}$ NOE connectivities, and the up-field Hα chemical shift and down-field Cα chemical shift values with respect to random-coil values indicate that the JM-A segment has a significant population in the helical conformation throughout the length of the peptide

(Wishart et al., 1992; Wüthrich, 1996). Isolated peptide fragments that form transient α–helices in solution are expected to be α–helical in the intact protein (Dyson et al., 1992).

The shift in the apparent K_D for JM-kinase dimerization from ~200 nM to >8 μM upon deletion of the JM-A segment suggests that the K_D for dimerization of the JM-A segment alone is ~2 mM or lower, assuming additivity. TOCSY spectra were acquired for the peptide at concentrations of 0.2 mM, 0.5 mM and 2 mM peptide under identical conditions. We observed concentration dependent line broadening for the methyl groups of leucine and valine (Figure S2E). The preferential line broadening of the Val and Leu methyl group resonances at higher concentration is consistent with concentration dependent oligomerization. These data cannot, however, be interpreted to give the nature or size of the oligomer formed.

NMR Structural Analysis of 35 Residue JM-A Peptide

We used ^{15}N- and ^{13}C-filtered nuclear Overhauser effect (NOE) experiments to look for close contacts between Leu 655, Leu 659 and Glu 663 in Segment A and other residues. Figure S7B shows a cross section of the upfield aliphatic region of the ^{15}N-^{1}H HSQC–NOESY spectrum. The amide proton of Leu 659 in Segment A shows two intra-residue NOEs with protons on Cβ and Cγ (labeled HB and HG, respectively), and an inter-residue NOE with protons on Cδ (HD) of Leu 655 in Segment B (which has a distinguishable chemical shift from Leu 655 in Segment A). The amide of Leu 655 in Segment A also shows intra-residue NOEs with its HB and HG, and an inter-residue NOE with the adjacent residue, Thr 654 HG (Figure S7B), but no long range NOE. The absence of the intra-residue NH–HD NOE for Leu 655 shows that crosspeaks are not

observed for distances of ca. 4.5 Å. This supports the assignment of the observed NOE between Leu 655 HD and Leu 659 NH as inter-residue rather than as intra-residue NH to HD for Leu 659, which would be at very similar chemical shifts.

Figure S7C shows a selected aliphatic region of a ^{13}C-^{1}H HSQC – NOESY spectrum. Intra-residue and long range NOEs are observed for Glu 663 in Segment A. The HG protons of Glu 663 show intra-residue NOEs with the HA and HB protons. There are two long range NOEs observed between the HG protons of Glu 663 and the HB and HD protons of Lys 652 in Segment B.

In summary, these NMR data indicate the presence of three close contacts involving the labeled residues. These involve (i) NH proton of Leu 659 in Segment A and the HD methyl group protons of Leu 655 in the other segment, (ii) the HG protons of Glu 663 in segment A and the HB and HD protons of Lys 652 in Segment B. There are no peaks supporting a close contact between the NH proton of Leu 655 in Segment A and protons in Segment B.

Figure 4D shows models for antiparallel and parallel helical dimers, based on coiled coil segments in the protein databank (the conclusions drawn depend primarily on the geometry of the backbone rather than the sequence of the particular structure used as a template). The close contacts inferred from the NOE data are consistent with an antiparallel model with the Leu 655 at the *d* position of the heptad repeat (left panel in Figure 4D). In this register of antiparallel helices, the NH group of Leu 655 is positioned away from the interfacial region, and the model does not predict close contacts with the methyl groups of leucine residues in the adjacent helix (open green circles in Figure 4D). This model has close interhelical contacts between the NH proton of Leu 659 in one helix

and the methyl groups of Leu 655 in the other helix, as well as between the sidechains of Glu 663 and Lys 652, consistent with the observed NOEs (closed green circles in Figure 4D).

In an antiparallel dimer with Leu 655 at the *a* position, the NH group of Leu 655 moves closer to the interfacial region, and a close contact with the methyl groups of Leu 658 of the other helix is predicted (closed red circles in the middle panel of Figure 4D) but a corresponding NOE is not observed. The model does predict the observed NOE between the NH proton of Leu 659 and the methyl groups of Leu 655 in the other helix (closed green circles in Figure 2B), but the sidechains of Glu 663 and Lys 652 are too far apart to explain the observed NOEs between these sidechains (open red circles in Figure 4D).

A parallel orientation is clearly inconsistent with the NMR data. For the register shown in the right panel in Figure 4D (with Leu 655 at the *d* position), a close contact is predicted between the NH proton of Leu 659 and the methyl groups of the same residue in the other helix (closed red circles in Figure 4D), but is not observed. The three close contacts inferred from the NOE data cannot be explained by a parallel model in either register.

Supplementary Figure Legends

Figure S1. The JM-kinase Construct Is Predominantly a Dimer in Solution (A) Dynamic light scattering of the His-tagged kinase core construct in solution. Molecular weight distribution of the single protein peak is plotted as squares against the elution volume. Reflective index and light scattering (at 90° to the incident beam) of the peak are

shown as solid and dashed lines, respectively. Data analysis using the program ASTRA 4.90.04 yielded a molecular weight of 40,000 Da, which corresponds to the monomeric state of kinase core. **(B)** Dynamic light scattering of the HIS-tagged JM-kinase construct in solution. The data collection and analysis was done as described in (A). The molecular weight of the predominant peak corresponds to 79,000 Da, which corresponds to the dimeric form of the JM-kinase domain (JM-kinase monomer has a molecular weight of 42,000 Da). Higher order oligomerization of the JM-kinase domain was also observed, as evidenced by the second peak corresponding to a 380,000 Da species. The nature of the higher oligomeric species of JM-kinase is unclear at present. In the absence of organization at the membrane (which restricts how many JM-A helices can form in a chain) the juxtamembrane latch may allow the formation of a chain of molecules, as observed in the Her4 crystal structure (Wood et al., 2008).

Figure S2. NMR Structural Analysis of the JM-A Peptide (A) Cross section of the d_{NN} region of the ^{1}H-^{1}H NOESY spectra of JM peptide (652-666) in 20 mM phosphate buffer pH 6.8, 10% D2O and 4% deuterated acetonitrile at 293K. **(B)** Summary of NOESY connectivities for the JM peptide. NOE connections shown in grey are ambiguous due to spectral overlap. **(C) and (D)** The plots of Hα and Cα chemical shift index against the residue number for the JMA-peptide are shown, respectively. **(E)** Plot of normalized intensity as function of concentration. The intensity for the methyl group of Leu 658, Leu 659, Leu 664, Val 665 and Leu 655 was normalized against T3Hγ intensity. The error was calculated from the signal/noise ration of the fit height. The ^{1}H-^{1}H TOCSY spectra were acquired with 0.2 mM (orange), 0.5 mM (red) and 2 mM (green) peptide under identical condition.

Figure S3. Transfection and Co-transfection Analysis of the Effects of Mutations in the LRRLL Motif on EGFR Autophosphorylation (A) Comparison of the effects of alanine and glycine substitutions in the JM-A segment. The first three panels compare activity of the full length wild type receptor with that for variants in which Arg 656 and Arg 657 are replaced by alanine and glycine. The next four panels shows results of co-transfection experiments using activator-impaired and receiver-impaired variants of the receptor, and compare the results of alanine and glycine substitutions in each variant. **(B)** Effects of mutations in the JM-A segment on Tyr 1173 phosphorylation. The level of EGF-stimulated phosphorylation relative to the wild type, after normalizing for EGFR levels, is shown below each lane.

Figure S4. Models of the Helical Parallel Dimer Between the JM-A Segments of EGFR (A) The modeled parallel JM-A dimers present two different helical packing scenarios: Leu655 placed in *a* position or in *d* position. The rotated views show ion pair interactions involving Arg 662. **(B)** Effect of mutations of the residues involved in ion pairs in the models of the parallel JM-A dimer (Arg 662) and the antiparallel JM-A dimer (Lys 652 and Arg 656). Phosphorylation at Tyr1173 was examined by immunoblotting of whole cell lysates with an anti-pY1173 antibody and the level of EGF-stimulated phosphorylation was normalized relative to the wild type. **(C)** Schematic diagrams of all combinations of heterodimeric parallel arrangement of JM-A helices between Her4 and EGFR or Her2. The unfavorable juxtaposition of the Glu residues in the parallel helical dimers is marked by red stars.

Figure S5. Model of the Helical Antiparallel JM-A EGFR Homodimer With Leu 655 at Position *a* Schematic diagram of the EGFR JM-A antiparallel helical homodimer with

Leu 655 placed at the *a* position. The electrostatic interactions between the charged residues are marked by the black dashed line. This arrangement does not provide a specific role for Arg 656 compared to the arrangement when Leu 655 is placed at the *d* position.

Figure S6. Models of Helical Antiparallel JM-A Dimers Between Her Family Members. Schematic diagrams of various combinations of antiparallel homo- and heterodimers of JM-A helices between Her family members. In all dimers, Leu 655 in EGFR and the corresponding residues in Her2, Her3 and Her4, were placed at the *d* position. All these arrangements lead to tight packing of the hydrophobic residues in the dimer interface and the favorable electrostatic interactions (dashed green lines) for each combination.

Figure S7. NMR Based Structural Analysis of 35 Residue JMA peptide (A) The JM-A peptide used for the NMR investigation is shown. The two JM-A segments are denoted as Segment-A and Segment-B, respectively. The residues highlighted with red stars (L655 and L659) in Segment-A are labeled with ^{15}N, and E663 in Segment-A, which is highlighted with green star, is double labeled with $^{15}N^{13}C$. **(B)** Aliphatic region of the 2D ^{15}N-^{1}H HSQC –NOESY spectra of the JM-A peptide in 50 mM deuterated Acetate buffer pH 5.1 10% D2O at 293K. The amino acid residues from Segment-A and Segment-B are denoted by suffixes A and B, respectively. **(C)** Upfield region of the 2D 13C-^{1}H HSQC – NOESY spectra of the JMA peptide.

Figure S8. Molecular Dynamics of the JM-A Helical Dimer Docked on the Kinase Domain (A) Overview of the structure used for molecular dynamics. **(B)** The stability of the hydrophobic and electrostatic interactions in the JM-A helical dimer in molecular

dynamics trajectories. The results of four independent trajectories, each extending for 10 ns, are shown. For each monitored ion pair, the distance between the penultimate carbon atoms of the two residues was calculated over the course of each trajectory, and ion pairs with distances smaller than a threshold value of 5Å were considered "intact". In order to quantify the hydrophobic packing of leucine residues in the helical dimer, the distance of the Cβ-atom of the leucine residue at the *a* position in one helix to the midpoint between the Cβ-atoms of two adjacent leucine residues at the *d* and *e* positions of the other helices (see Figure 4B in the main text) was computed and recorded as a function of time. Hydrophobic packing at a given time point was considered "intact" when this distance did not exceed its mean value (over the course of the entire trajectory) by more than 0.5 Å. The close packed configuration of the six leucine sidechains is stable in each of the simulations. The intramolecular and intermolecular ion pairs are broken and reformed due to transient interactions with water and ions, but are maintained on average (Figure S3B). These results suggest that the formation of an antiparallel helical dimer is a plausible model for the JM-A segments. In the diagram intact ion pairs and intact hydrophobic packing of leucine residues in the helical dimer between the helix of the receiver kinase (Rec) and the helix of the activator kinase (Act) is marked as green and a break in the interaction is marked as red.

Figure S9. The Surface Electrostatic Potential of the Inactive Dimer. Two representative views of the inactive dimer and the corresponding calculated surface electrostatic potentials are shown. The surface electrostatic potential was calculated using GRASP2 (Petrey and Honig, 2003).

Figure S10. The Effect of Mutations in the AP-2 helix. The effect of deletion **(A)** or

mutations **(B)** of residues in the AP-2 helix on EGFR autophosphorylation in COS7 cells was determined by immunoblotting of whole cell lysates with anti-pY1173 antibody. **(C)** Catalytic efficiency (k_{cat}/K_M) of the EGFR kinase core (672-998) and mutants of vesicles. Error bars correspond to the standard deviation of the linear fittings (Zhang et al., 2006).

Table S1

Data collection	
Beamline	ALS 8.2.2
Resolution (Å)	50-3.00 (3.12-3.00)
Space group	P21
Unit cell parameters	a=61.8 Å, b=72.4 Å, c=143.4 Å, β=101.7°
Content of the asymmetric unit	four kinase domains in complex with AMP-PNP
R_{merge}	15.8 (53.0)
I/σ(I)	7.0 (1.3)
Completeness	94.5 % (79.2%)
Multiplicity	3.4 (2.8)
Refinement	
Unique reflections	24429
R_{work}/R_{free}	21.4/28.7
No. of protein atoms	9778
No. of AMP-PNP atoms	128
Water molecules	35
r.m.s. deviation from ideality in bond lengths (Å)	0.004
r.m.s. deviation from ideality in bond angles (°)	0.786

**Numbers in parentheses refer to the highest resolution shell*

Table S2

Protein	In solution	
	Protein [μM]	Peptide [μM]
kinase core	14	100, 200, 400, 600, 800
kinase core L834R	3.5	100, 200, 400, 600, 800
645-998	3.5	100, 200, 400, 600, 800
658-998	3.5	100, 200, 400, 600, 800
645-998 V924R	7	100, 200, 400, 600, 800
645-998 I682Q	7	100, 200, 400, 600, 800
658-998 V924R	7	100, 200, 400, 600, 800
658-998 I682Q	7	100, 200, 400, 600, 800
645-998 V924R & 658-998 I682Q	7	100, 200, 400, 600, 800
645-998 V924R & 658-998 I682Q	7	100, 200, 400, 600, 800
658-998 V924R & 658-998 I682Q	7	100, 200, 400, 600, 800

Protein	Attached to vesicles	
	Protein [μM]	Peptide [μM]
kinase core	7	50, 100, 200, 300, 400
kinase core L834R	3.5	50, 100, 200, 300, 400
kinase core F973R	7	50, 100, 200, 300, 400
kinase core AP-2 helix deletion	7	50, 100, 200, 300, 400

References

Case, D. A., Darden, T. E., Cheatham, T. E., Simmerling, C. L., Wang, J., Duke, R., Luo, R., Merz, K. M., Pearlman, D. A., Crowley, M.*, et al.* (2006). AMBER 9. In University of California, San Francisco.

Cornell, W. D., Cieplak, P., Bayly, C. I., Gould, I. R., Merz, K. M., Ferguson, D. M., Spellmeyer, D. C., Fox, T., Caldwell, J. W., and Kollman, P. A. (1995). A 2nd Generation Force-Field for the Simulation of Proteins, Nucleic-Acids, and Organic-Molecules. Journal of the American Chemical Society *117*, 5179-5197.

Cornell, W. D., Cieplak, P., Bayly, C. I., Gould, I. R., Merz, K. M., Ferguson, D. M., Spellmeyer, D. C., Fox, T., Caldwell, J. W., and Kollman, P. A. (1996). A second generation force field for the simulation of proteins, nucleic acids, and organic molecules (vol 117, pg 5179, 1995). Journal of the American Chemical Society *118*, 2309-2309.

Darden, T., York, D., and Pedersen, L. (1993). Particle Mesh Ewald - an N.Log(N) Method for Ewald Sums in Large Systems. Journal of Chemical Physics *98*, 10089-10092.

Dyson, H. J., Merutka, G., Waltho, J. P., Lerner, R. A., and Wright, P. E. (1992). Folding of peptide fragments comprising the complete sequence of proteins. Models for initiation of protein folding. I. Myohemerythrin. J Mol Biol *226*, 795-817.

Goddards, T. D., and Kneller, D. G. Sparky 3.111. University of California, San Francisco.

Pearlman, D. A., Case, D. A., Caldwell, J. W., Ross, W. S., Cheatham, T. E., Debolt, S., Ferguson, D., Seibel, G., and Kollman, P. (1995). Amber, a Package of Computer-Programs for Applying Molecular Mechanics, Normal-Mode Analysis, Molecular-Dynamics and Free-Energy Calculations to Simulate the Structural and Energetic Properties of Molecules. Computer Physics Communications *91*, 1-41.

Petrey, D., and Honig, B. (2003). GRASP2: visualization, surface properties, and electrostatics of macromolecular structures and sequences. Methods Enzymol *374*, 492-509.

Ryckaert, J. P., Ciccotti, G., and Berendsen, H. J. C. (1977). Numerical-Integration of Cartesian Equations of Motion of a System with Constraints - Molecular-Dynamics of N-Alkanes. Journal of Computational Physics *23*, 327-341.

Wishart, D. S., Sykes, B. D., and Richards, F. M. (1992). The chemical shift index: a fast and simple method for the assignment of protein secondary structure through NMR spectroscopy. Biochemistry *31*, 1647-1651.

Wood, E. R., Shewchuk, L. M., Ellis, B., Brignola, P., Brashear, R. L., Caferro, T. R., Dickerson, S. H., Dickson, H. D., Donaldson, K. H., Gaul, M.*, et al.* (2008). 6-Ethynylthieno[3,2-d]- and 6-ethynylthieno[2,3-d]pyrimidin-4-anilines as tunable covalent modifiers of ErbB kinases. Proc Natl Acad Sci U S A *105*, 2773-2778.

Wüthrich, K. (1996). NMR of proteins and nucleic acids. Wiley, John & Sons, Inc.

Young, M. A., Gonfloni, S., Superti-Furga, G., Roux, B., and Kuriyan, J. (2001). Dynamic coupling between the SH2 and SH3 domains of c-Src and hck underlies their inactivation by C-terminal tyrosine phosphorylation. Cell *105*, 115-126.

Zhang, X., Gureasko, J., Shen, K., Cole, P. A., and Kuriyan, J. (2006). An allosteric mechanism for activation of the kinase domain of epidermal growth factor receptor. Cell *125*, 1137-1149.

Figure S1, Jura et al.

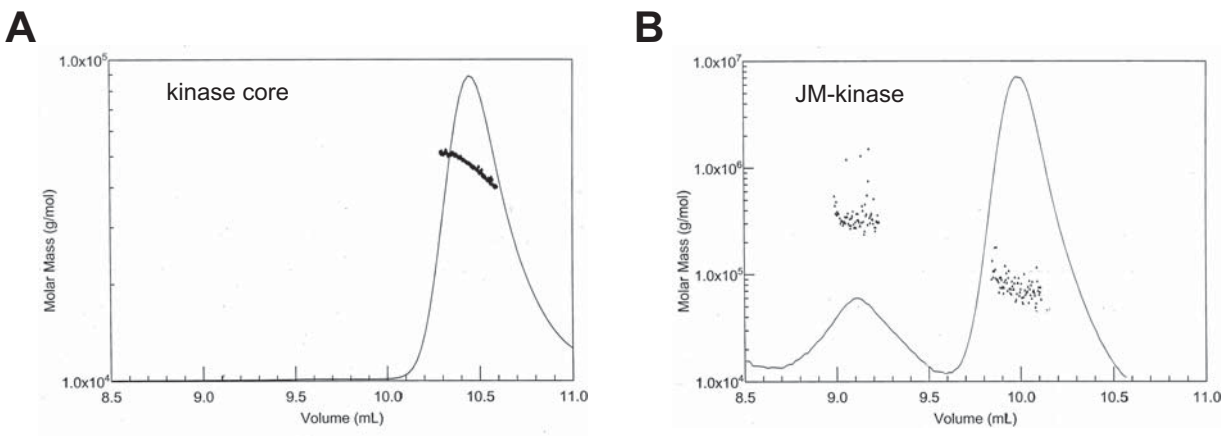

Figure S2, Jura et al.

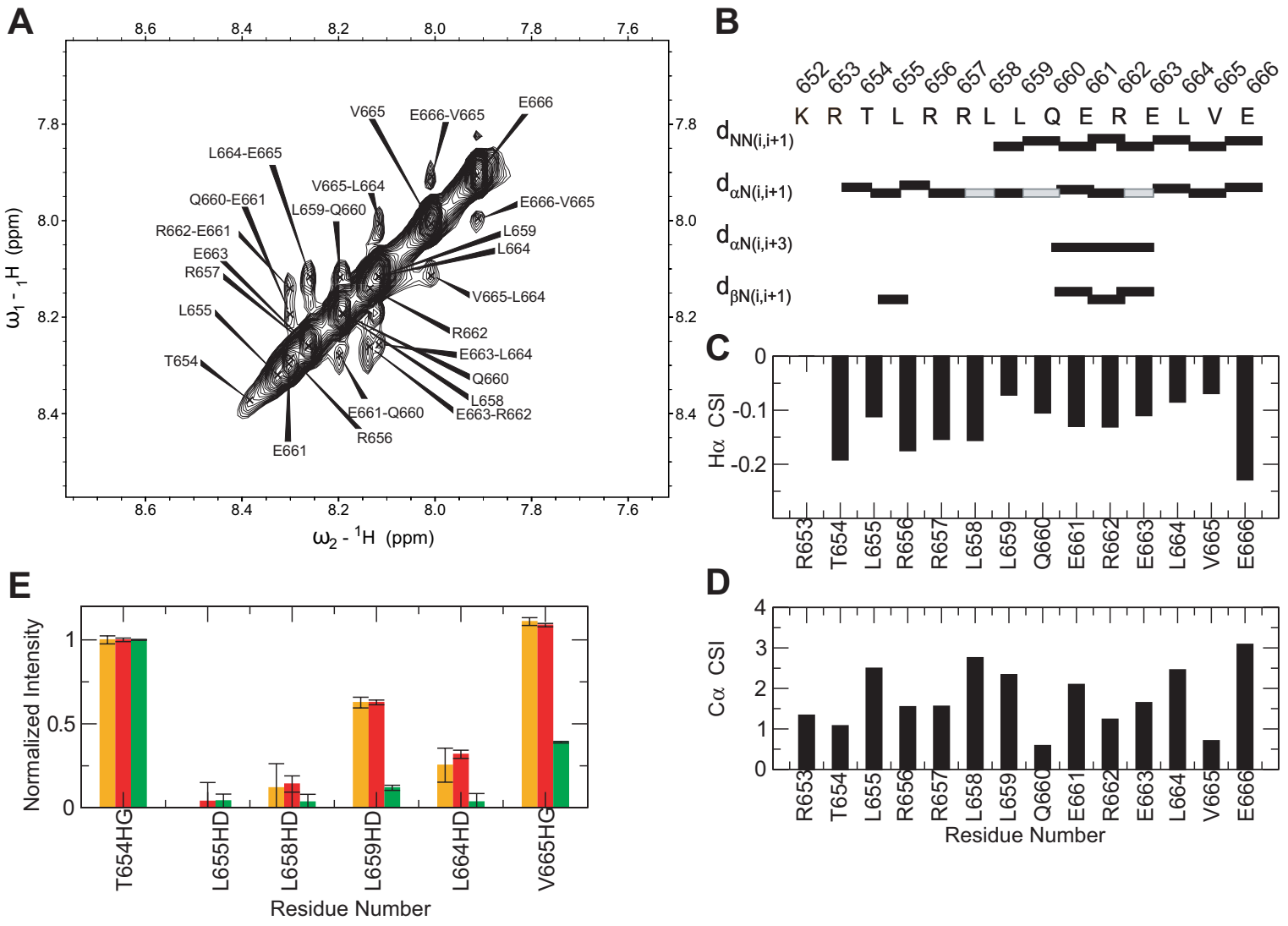

Figure S3, Jura et al.

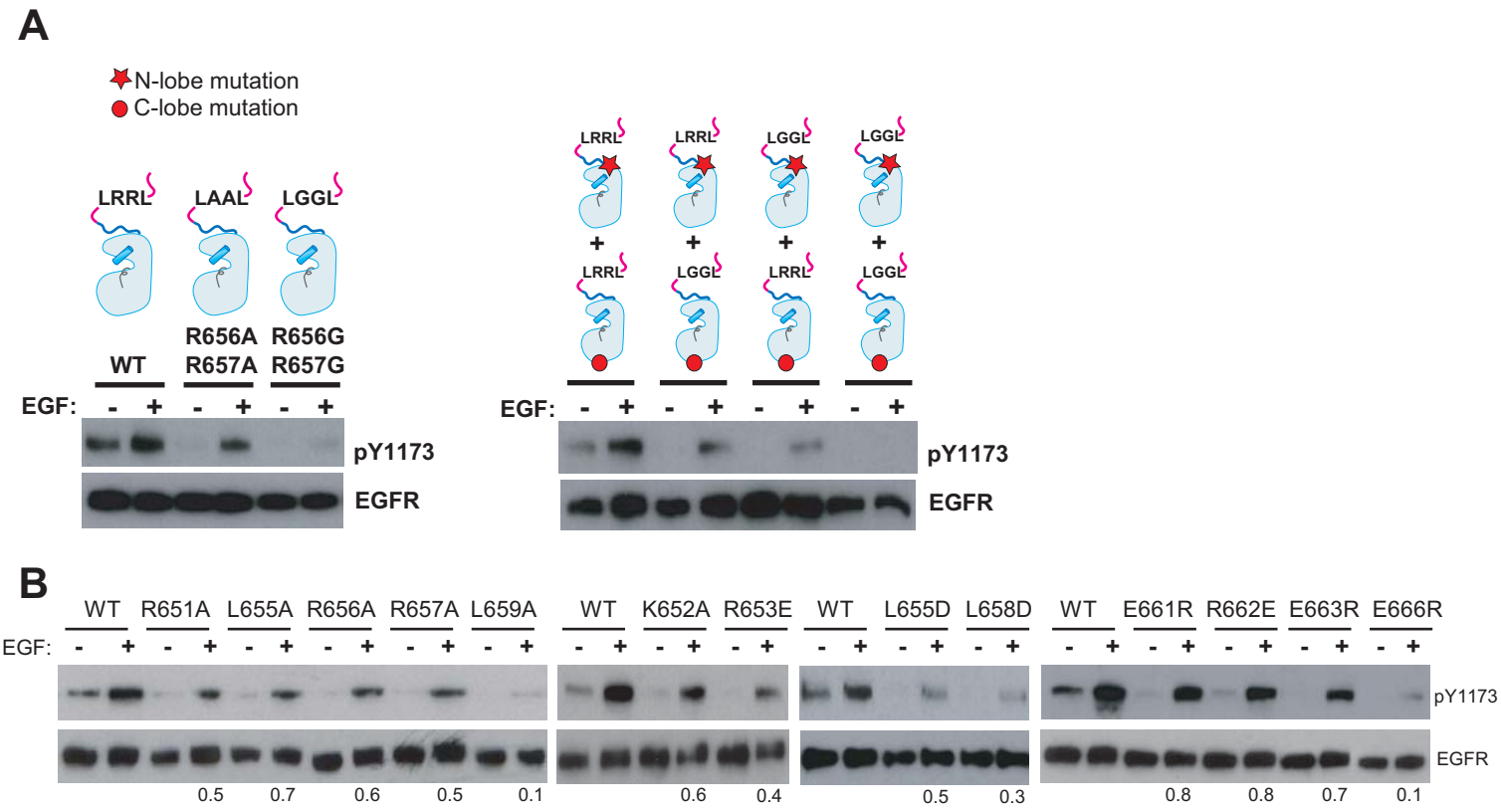

Figure S4, Jura et al.

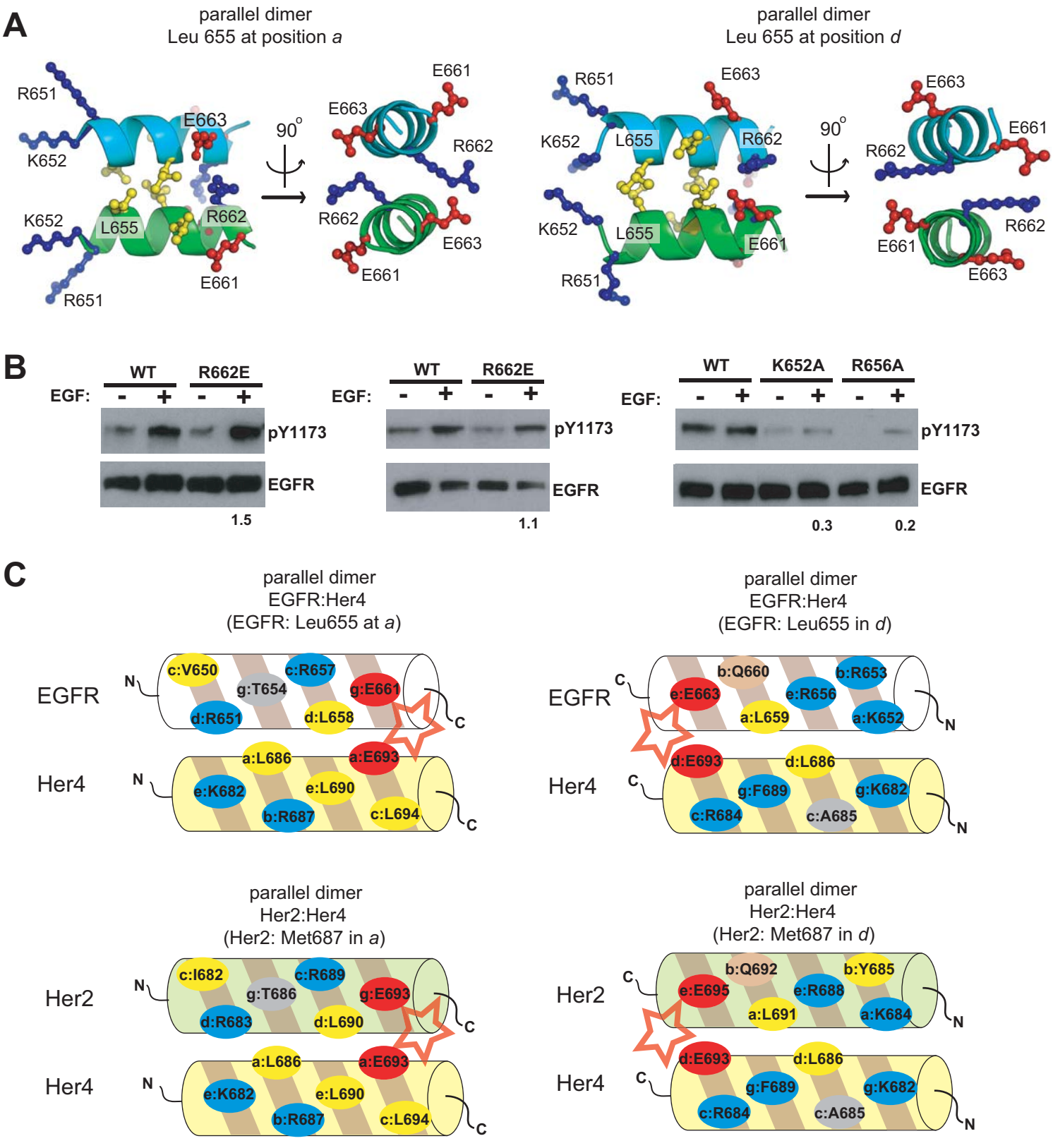

Figure S5, Jura et al.

antiparallel dimer
EGFR:EGFR
(L655 at position *a*)

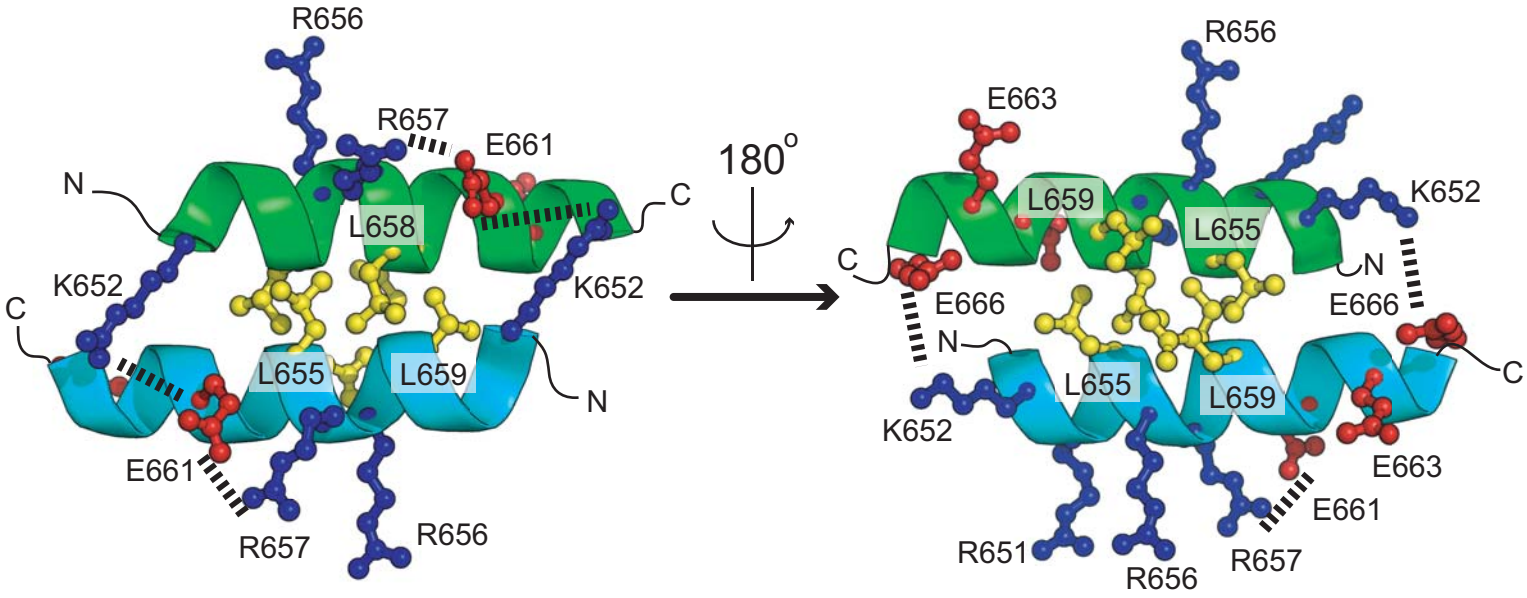

Figure S6, Jura et al.

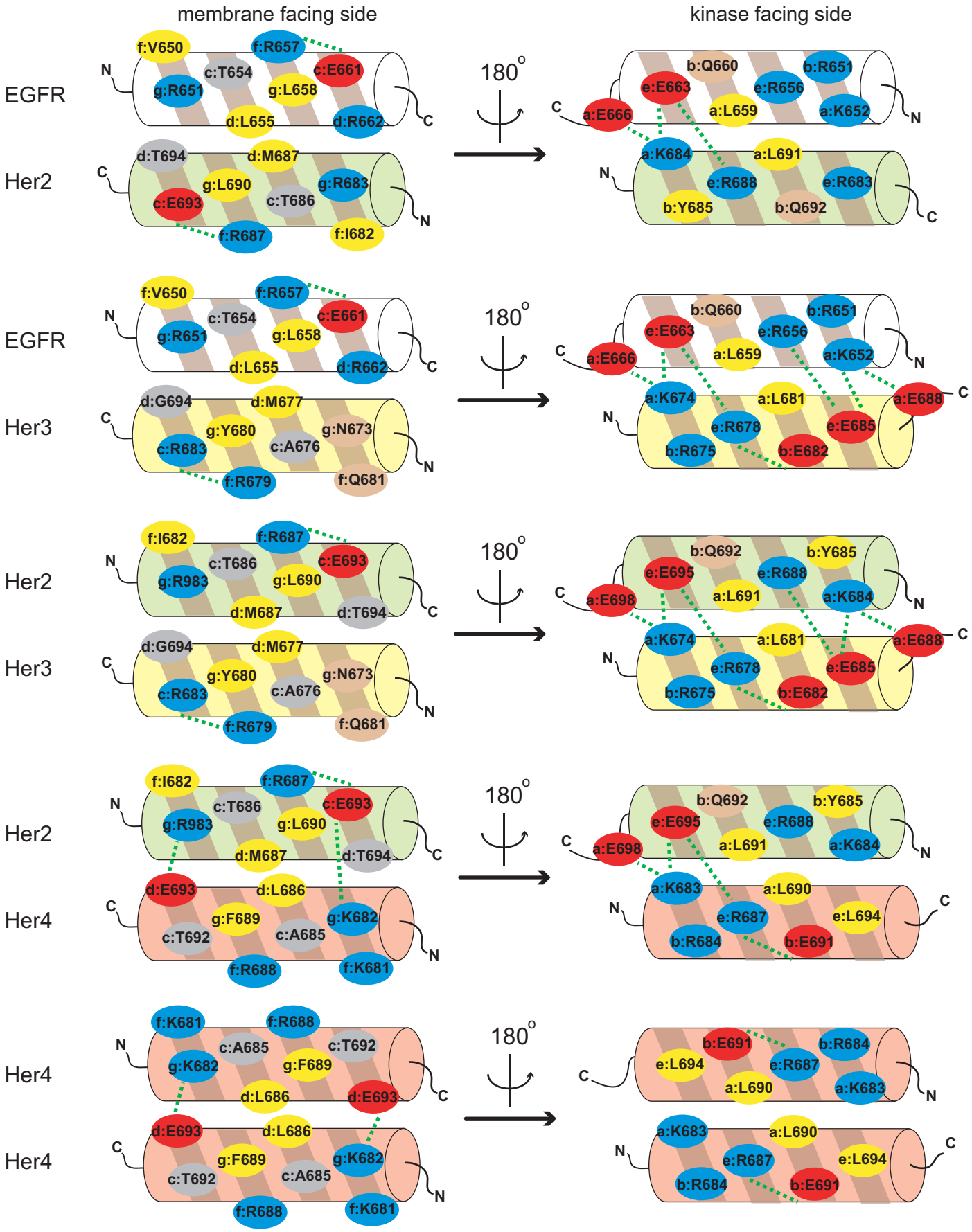

Figure S7, Jura et al.

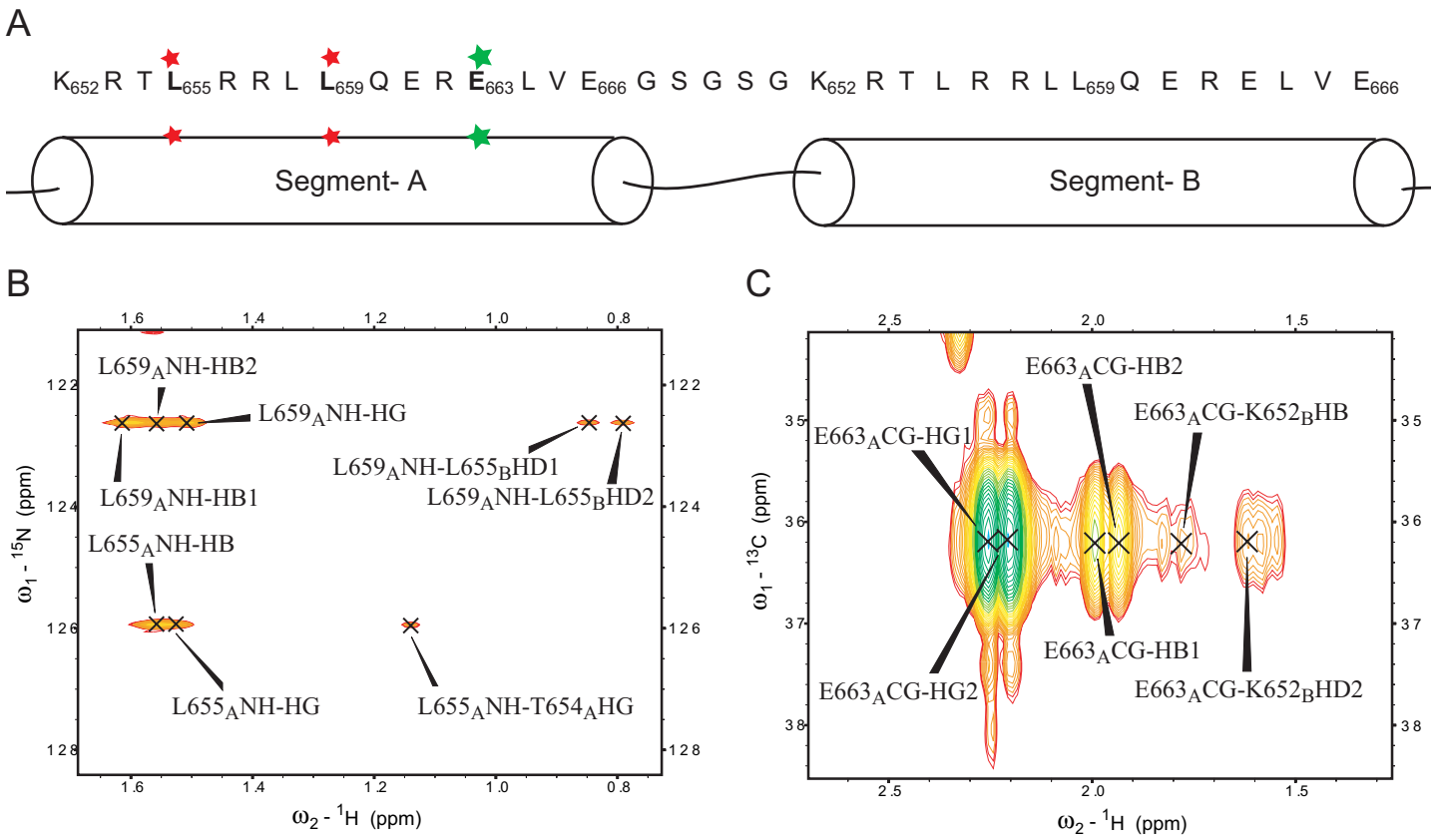

Figure S8, Jura et al.

A

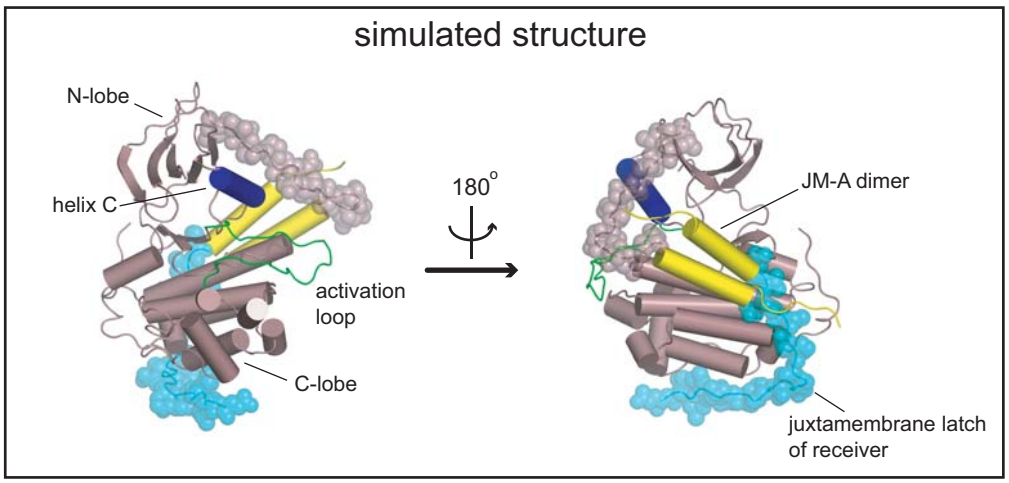

B

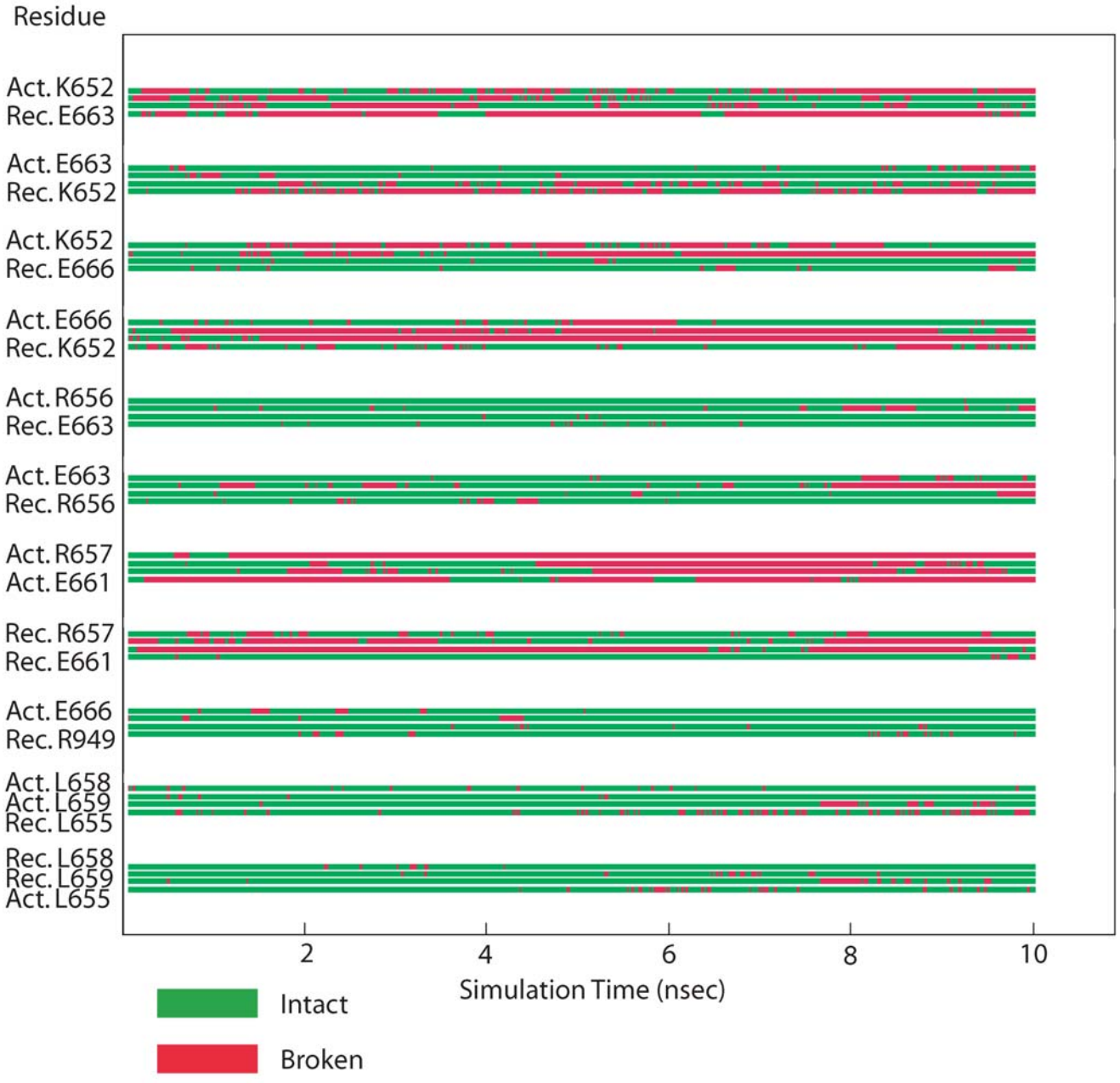

Figure S9, Jura et al.

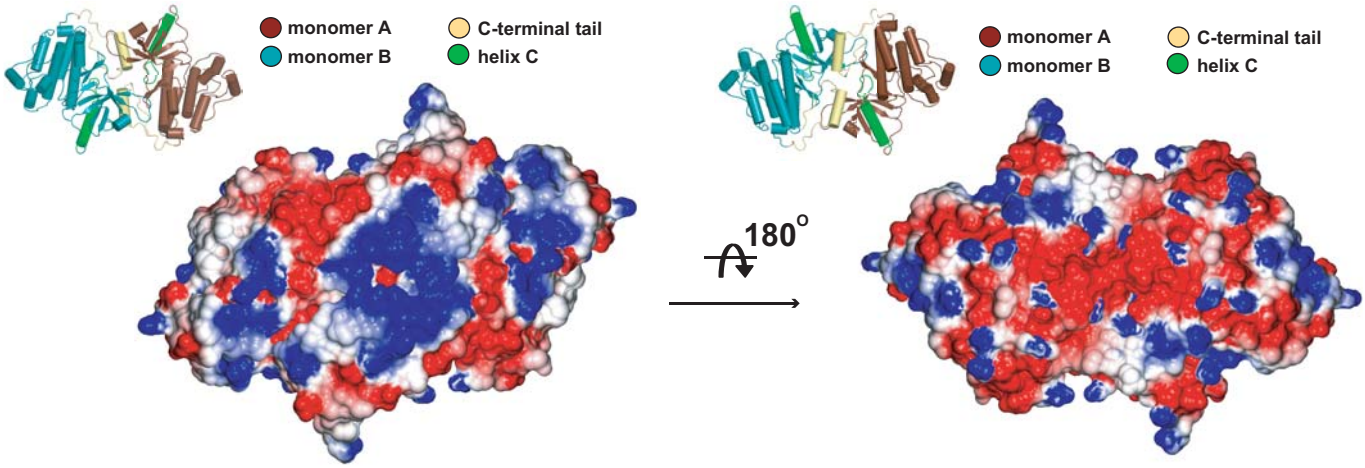

Figure S10, Jura et al